JOURNAL OF CATALYSIS 140, 262–280 (1993)

# The Kinetics of Hydrocarbon Cracking

## The Cracking of *n*-Nonane

W. A. GROTEN AND B. W. WOJCIECHOWSKI[1]

*Department of Chemical Engineering, Queen's University, Kingston, Ontario, Canada K7L 3N6*

Received February 25, 1992; revised November 10, 1992

A general kinetic model which describes the catalytic cracking of pure hydrocarbons is presented. The model includes a monomolecular cracking path based on the Langmuir adsorption isotherm as well as a bimolecular path, following Rideal kinetics, which accounts for the possibility of a chain cracking mechanism being involved. Catalyst decay is accounted for using the time-on-stream decay function. Fitting of experimental data from *n*-nonane cracking on USHY at 673 K, combined with Monte Carlo simulations indicates that, in that case, the total catalytic activity could include between 0 and 90% of activity due to chain processes. This large margin of error stems from the combined effects of a large decay rate, forcing the experimenter to use average conversion data, and of experimental error. Fitting of the model to previously published cracking data for 2-methylpentane on USHY showed that the model lacks a suitable parameter to account for thermal reactions which were not accounted for in the original data set. This observation supports the impression that the model is sensitive to departures from the postulated mechanism. The above kinetic model has also been fitted to the results of *n*-nonane cracking at three temperatures as well as to previously published data for various other linear paraffins. In all these systems the parameter $A_2$, which is a function of the bimolecular cracking rate constants, is found to be statistically insignificant, in spite of other experimental evidence which supports the existence of this route of cracking. Parametric analysis of the *n*-nonane conversion results suggests that catalyst surface composition is very sensitive to temperature due to a large difference in the enthalpy of adsorption between the reactant and the average product of cracking. As temperature is increased, the reactant competes more successfully for active sites, with the result that the relative importance of monomolecular cracking processes increases with temperature at the expense of bimolecular reactions. The rate of cracking per crackable bond was also considered. We present arguments that previous reports of increased cracking rate per bond as chain length of the feed molecule is increased are due to the use of inadequate models of the kinetics involved, rather than constituting a real phenomenon. 

## INTRODUCTION

Mechanistic studies of catalytic cracking on zeolites have suggested that two modes of reaction are required to explain the product distribution observed: monomolecular protolysis on pristine Brønsted acid sites on the zeolite framework and bimolecular reactions between an adsorbed carbenium ion and a gas-phase reactant molecule (*1–4*). The latter mechanism constitutes a bimolecular reaction between an adsorbed product of cracking and gas-phase molecule of the feed (*4, 5*) and is the "chain" mechanism of cracking. While evidence from various experimental studies in the literature suggests cracking occurs via both mechanisms, their quantitative importance to the overall kinetics has not been rigorously assessed. Previously, the kinetics of *n*-hexadecane cracking (*6–8*) and of other linear paraffins in the $C_6$–$C_{16}$ range (*4, 9–11*) was modelled assuming a monomolecular process and a Langmuir isotherm, as well as with a simpler first-order model (*12*). McVicker *et al.* (*13*) proposed an entirely different kinetic model for the reaction of isobutane based on the reaction being

[1] To whom correspondence should be addressed.



0021-9517/93 $5.00

propagated via surface-stabilized radicals. With the general acceptance of surface carbocations as the intermediates in catalytic cracking, this model has not been given further elaboration in the literature.

Both the monomolecular Langmuir-based model and the simple first-order model have been used to support mechanistic conclusions about the cracking reaction. At the same time, it has been shown in other studies (*1, 2, 13, 14*) that a chain cracking reaction is important with $C_4$ paraffins. Furthermore, Abbot and Wojciechowski (*9*) presented experimental data from the cracking of various branched $C_6$ paraffins in which an induction period in the conversion versus time-on-stream curves was clearly visible. Bimolecular reactions have also been shown to be important in the reactions of olefins (*15*) on USHY and to a lesser extent with cumene (*5*) on various solid-acid catalysts.

In this work the simpler models previously used to describe hydrocarbon cracking kinetics are elaborated to yield a new model which includes the possibility of cracking via a chain mechanism. Decay is accounted for using the time-on-stream approach to decay (*5, 16*). A simpler model involving both monomolecular and bimolecular cracking was recently proposed by Haag *et al.*, who did not take into account catalyst decay. That model is also accommodated by this, more general approach (*17*). Our general model therefore encompasses all earlier monomolecular models presented in the literature and accommodates most of the currently discussed mechanisms of catalytic cracking. The model is examined using simulation in order to show what conditions may allow us to discriminate between the various mechanisms of cracking on the basis of kinetics alone and to investigate the morphology of the model. Experimental data from a study of *n*-nonane cracking and previously published data for the cracking of various other paraffins on USHY are used to evaluate the model's ability to fit experimental data.

## THEORY

The assumptions involved in the development of the general model are:

- all cracking reactions are irreversible,
- surface reactions are rate limiting.

The initiating monomolecular reaction involves the adsorption of the reactant as a carbonium ion followed by protolysis, resulting in the formation of a gas-phase paraffin and a residual surface carbenium ion. The residual surface ion can desorb to form an olefin product or undergo a bimolecular reaction with a second gas-phase reactant molecule. A simplified scheme of kinetically important reactions can be represented by

$$A + S \overset{K_A}{\leftrightarrows} AS \xrightarrow{\Sigma k_{M_i}} n_i P_i + S \qquad (1)$$

$$P_i + S \overset{K_{P_i}}{\leftrightarrows} P_i S \xrightarrow[(\Sigma k_{C_j})_i]{A} n_i P_i + S, \qquad (2)$$

where A is the reactant, $P_i$ the $i$th product, S an active site on the catalyst, $K_A$, $K_{P_i}$ are the equilibrium adsorption constants for the reactant, A, and the $i$th product, respectively, $\Sigma k_{M_i}$ is the sum of the rate constants for the various modes of the monomolecular cracking, while $(\Sigma k_{C_j})_i$ is the sum of the rate constants for the bimolecular reaction between the $i$th surface species and the reactant, and $n_i$ is the stoichiometric factor for the formation of the $i$th product.

A differential rate expression is obtained by assuming that the surface reactions are rate-limiting and that all adsorption reactions are at equilibrium. Thus the surface concentrations of adsorbed reactant and products can be expressed as

$$[AS] = K_A[S][A]; \qquad (3)$$

$$[P_iS] = K_{P_i}[P_i][S]. \qquad (4)$$

The expression governing the time rate of change in A will be

$$-r_A = \left(\sum k_{M_i}\right)[AS] + \left(\sum_i \left(\sum_j k_{C_j}\right)_i [P_iS]\right)[A]. \qquad (5)$$

Using Eqs. (3) and (4) to substitute for the surface concentrations in (5) gives

$$-r_A = \left(\sum k_{M_i}\right)K_A[A][S] + \left(\sum_i \left(\sum_j k_{C_j}\right)_i K_{P_i}[P_i]\right)[A][S], \quad (6)$$

Next, a site balance is carried out on the active sites. There are three possible states in which a site may exist: in a pristine state, free of adsorbed species; with an adsorbed reactant or product of reaction on it; or it may be deactivated. It is assumed that the sites decay according to the time-on-stream function. If subscripts 0 and d represent initial sites and deactivated sites, respectively, then a balance on the sites gives

$$[S] = [S]_0 - [AS] - \sum_i [P_iS] - [S]_d \quad (7)$$

$$[S] = [S]_0 - \left[K_A[A] + \sum_i K_{P_i}[P_i]\right][S] - [1 - (1 + Gt)^{-N}][S]_0, \quad (8)$$

where $(1 + Gt)^{-N}$ is the fraction of sites still active at time $t$.

Solving for [S] and substituting into (6) results in

$$-r_A = \frac{[(\sum k_{M_i})K_A[A] + (\sum_i(\sum_j k_{C_j})_i K_{P_i}[P_i])[A]][S]_0(1 + Gt)^{-N}}{1 + K_A[A] + \sum K_{P_i}[P_i]}. \quad (9)$$

It is assumed that the concentrations of product species, $[P_i]$, involved in the bimolecular cracking and competitive adsorption reactions are proportional to the conversion of reactant thus:

$$[P_i] = \mathcal{F}_i([A]_0 - [A]),$$

where $\mathcal{F}_i$ represents the moles of the ith product formed per mole of feed reacted, i.e., the molar selectivity. This is equivalent to assuming that all products are primary and stable. Such a simplification is quite accurate up to some 50% conversion in the systems under consideration here and becomes inapplicable above some 75% conversion. The molar selectivity of the ith product is the sum over all reactions of the probablity $S_j$, for each reaction, times the stoichiometric factor for the production of $i$ in this $j$th reaction, $n_j$. Thus,

$$\mathcal{F}_i = \sum_j (S_j n_j).$$

Summing over all $i$ products gives

$$\sum_i \sum_j (S_j n_j)_i = \sum_i \mathcal{F}_i = 1 + \varepsilon,$$

where $\epsilon$ is the volume expansion coefficient for the reaction and is assumed to be constant with respect to conversion. This parameter is experimentally determined using initial selectivity data.

It is convenient to express the concentration of reactant in terms of the dimensionless variable $X$, the fractional conversion of the reactant:

$$[A] = [A]_0 \frac{(1 - X)}{(1 + \varepsilon X)} = C_{A_0} \frac{(1 - X)}{(1 + \varepsilon X)}.$$

The reactions under consideration here are normally carried out in plug-flow reactors. Recall that the design equation for a plug-flow reactor is (*19*).

$$-r_A = C_{A_0} \frac{dX}{d\tau},$$

where $\tau$ is the space time and is proportional to $P$, the ratio of the weight of catalyst in the bed to the total weight of reactant passed over the catalyst, and to $t_f$ is the run duration ($\tau \alpha P t_f$). The constant of proportionality was arbitrarily assigned a value of one for this work.

Using these relationships and Eq. (9),

gives

$$\frac{\partial X}{\partial \tau} = \frac{[A_1[(1 - X)/(1 + \varepsilon X)] + A_2[(1 - X)/(1 + \varepsilon X)]^2][1 + Gt]^{-N}}{1 + B[1 - X)/(1 + \varepsilon X)]}, \tag{10}$$

where

$$A_1 = \frac{(\Sigma\, k_{M_i})K_A + (\Sigma_i\, (\Sigma_j\, k_{C_j})_i K_i \mathcal{F}_i)C_{A_0}}{1 + \Sigma\, K_i \mathcal{F}_i C_{A_0}}\,[S]_0 \tag{11}$$

$$A_2 = \frac{-(\Sigma_i\, (\Sigma_j\, k_{C_j})K_i \mathcal{F}_i)C_{A_0}}{1 + \Sigma\, K_i \mathcal{F}_i C_{A_0}}\,[S]_0 \tag{12}$$

$$B = \frac{(K_A - (\Sigma_i\, K_i \mathcal{F}_i))C_{A_0}}{1 + \Sigma_i\, K_i \mathcal{F}_i C_{A_0}} \tag{13}$$

where $G$ = decay constant, $N$ = decay exponent, and the parameters are restricted to the following regions:

$$A_1 > 0; \quad -A_1 < A_2 \leq 0; \quad B > -1;$$

$$G \geq 0; \quad N \geq 0.$$

The above model can be used to describe a first order kinetic process if $A_2$ and $B$ are equal to zero. There are two possible adsorption scenarios which lead to $B = 0$; when the surface is sparsely covered with both reactant and product ($K_A \simeq 0$ and $\Sigma\, K_i \mathcal{F}_i \simeq 0$) or when a singularity occurs, that is if $K_A = \Sigma\, K_i \mathcal{F}_i$. The sparse coverage condition represents the typical low pressure condition of heterogeneous catalysis (*18*). The second case can be understood if one imagines a simple cracking reaction where only 2 products are formed ($\mathcal{F}_1 = \mathcal{F}_2 = 1$). The singularity then occurs when $K_A = K_1 + K_2$. In that case, the ratio of the fraction of the surface covered by reactant, $\theta_A$, to that by the products, $\theta_1 + \theta_2$, will be the same as the ratio of their mole fractions in the gas phase. Under these conditions the observed kinetics are identical to those of a homogeneous gas-phase reaction, since adsorption effects do not distort the relative concentrations of the adsorbed reactant and products from their gas-phase concentrations.

The model describes monomolecular cracking kinetics following the Langmuir adsorption isotherm when $A_2$ is zero. Both bimolecular and monomolecular cracking with competitive adsorption for active sites is described by the full model. Statistical model building can now be applied and the simplest model which adequately describes the kinetic data selected.

The rate expression contains two independent variables, $t$, the catalyst age, and $\tau$, space time. In a plug flow reactor system, each differential increment of reactant is in contact with the catalyst for a time $d_\tau$ which is much smaller than the total run during $t_f$. Therefore, it is assumed that each differential element of reactant contacts catalyst of the same age along the length of the reactor. With this assumption, the rate expression can be integrated with respect to space time, treating catalyst age as constant. The time-on-stream dimension is dealt with subsequently. The validity of the time-on-stream model has been discussed previously (*16*) and depends on assuming that both reactant and products are equally likely to cause a deactivation event to occur.

Rearranging Eq. (10) to separate the variables gives

$$\frac{a + bX + cX^2}{(pX + q)(1 - X)}\,dX = (1 + Gt)^{-N} d\tau, \tag{14}$$

where

$$a = 1 + B, \quad b = 2\epsilon + B(\epsilon + 1), \quad c = \epsilon(\epsilon - B),$$
$$q = A_1 + A_2, \quad p = A_1\epsilon - A_2.$$

Integration of Eq. (14) within the limits $X = 0$, $X = X_f$; $\tau = 0$, $\tau_f$ and with t constant gives the following implicit equation in instantaneous output conversion, $X_f$:

$$\phi_1 X_f + \phi_2 \ln(1X_f) + \phi_3 \ln(\phi_4 X_f + 1) + \phi_5 \tau_f (1 + Gt)^{-N} = 0, \quad (15)$$

where $\phi_i$ are functions of the constant parameters. When the kinetic parameters are restricted to regions of physical significance as outlined above there is only one set of $\phi_i$ possible as shown below:

$$\phi_1 = -p(p + q)\epsilon(\epsilon - B)$$
$$\phi_2 = -p^2(1 + \epsilon)^2$$
$$\phi_3 = p^2(1 + B) - pq(2\epsilon + B(\epsilon - 1)) + q^2(\epsilon - B)\epsilon$$
$$\phi_4 = p/q$$
$$\phi_5 = -p^2(p + q).$$

$p$, $q$ are defined for Eq. (14).

The roots of Eq. (15) predict the instantaneous conversion at the exit of the reactor as a function of catalyst age, $t$. Because catalyst decay is often rapid in cracking systems, it is not possible to measure instantaneous conversion $X_f$. To circumvent this problem, the products and unconverted reactant are pooled during the time $t = 0$ to $t_f$ and the average conversion measured. This process can be described mathematically by

$$\bar{X}_f = \frac{1}{t_f} \int_0^{t_f} X_f \, dt, \quad (16)$$

where $\bar{X}_f$ is the time averaged conversion obtained in a run of duration $t_f$.

The expression for $X_f$, Eq. (15), is an implicit equation, and to obtain values of $\bar{X}_f$ the integration must be carried out numerically. Fortunately, $X_f$ can be determined from Eq. (15) to an arbitrary degree of accuracy using an appropriate root finding routine. The numerical integration in Eq. (16) then becomes relatively straight forward. Brent's method (*20*) was used to determine the roots while a five-step Gaussian quadrature was applied for the subsequent numerical integration of Eq. (16). Simulations with quadrature rules of various orders and step control policies resulted in convergence to the same value as reaction time became large for any set of parameters, or if the step size was chosen small enough for a fixed reaction time (*21*). In treating experimental data, the optimal parameters of the model were determined by minimizing the sum of squares of residuals between the experimental average conversion and that predicted by numerical integration of Eq. (16). The Levenburg–Marquardt approach was used with subroutines published by Press *et al.* (*22*).

## EXPERIMENTAL

### *Catalyst Activation*

NaY catalyst which we modified to form the USHY used in this study was purchased from BDH Chemicals (Lot No. 45912, 13Y, SK40). The chemical composition of the parent NaY is given in Table 1. About 75 grams of the NaY (dried under vacuum at 383 K) was stirred with 500 ml of 0.5 *M* $NH_4NO_3$ for 24 h at room temperature. The solids were removed from the

TABLE 1

Chemical and Physical Properties NaY (Anhydrous)

| | |
|---|---|
| Oxygen | 48.14 wt% |
| Silicon | 29.68 |
| Aluminum | 12.44 |
| Sodium | 9.64 |
| Chlorine | 0.05 |
| Fluorine | 0.05 |
| Bulk ratio Si/Al | 2.29 |
| $^{29}$Si MAS-NMR Si/Al | 2.42 |
| Unit cell constant | 24.696 Å |
| $N_2$ BET surface area ($m^2/g$) | 590 |

electrolyte by filtering through a 5-μm filter. The cake was then washed with distilled water to remove electrolyte. The solid was next dried and calcined in a static oven at 773 K for 2 h. This exchange, drying and calcining was repeated 10 times, resulting in a 99+% exchanged HY catalyst. The final powder was pelletized to form particles of between 80 and 100 mesh size, then steamed for 24 h at 473 K to form the final catalyst.

All catalytic runs were carried out in an isothermal plug-flow reactor (*5*).

## RESULTS AND DISCUSSION

### *Examination of the Model by Simulation*

We first explore the morphology of our kinetic equation using the following simulations based on a hypothetical cracking reaction of "A" into two products, $P_1$ and $P_2$. The volume expansion coefficient, $\epsilon$, was taken as one, while $\Sigma K_i \mathcal{F}_i = K_{P_1} + K_{P_2} = 2K_P$. The simulations were performed in order to examine the influence of adsorption, decay, and reaction mechanism on the morphology of plots of fractional average conversion against time on stream along contours of constant catalyst-to-reactant ratio. To simplify the analysis further, it is assumed that the system is such that $\Sigma K_i \mathcal{F}_i C_{A_0}$ is much larger than one (high-pressure assumption for product adsorption reactions) and that $C_{A_0}$ is equal to 1. Furthermore we use the rate expression derived on the basis of assuming that an equilibrium exists between product olefins and corresponding carbenium ions. Under these conditions, the parameters of the model can be simplified to

$$A_1 = (K_A/(2K_P))k_M + k_C$$

$$A_2 = k_C$$

$$B = (K_A/(2K_P)) - 1.$$

All the rate constant terms here include the initial concentration of sites. The decay parameters, $G$ and $N$, were assigned values of one for all simulations except where noted.

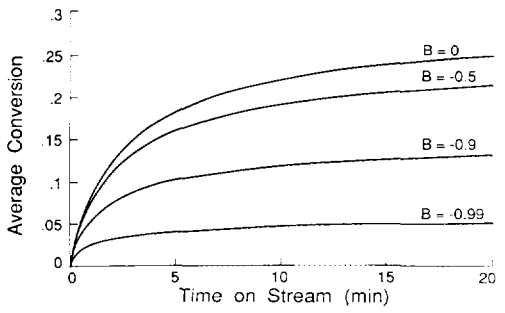


FIG. 1. Monomolecular model simulations: adsorption effects; $B$ as indicated, $k_M = 1$, $G = 1$ [time$^{-1}$]; $N = 1$; $\epsilon = 1$; catalyst/reactant = 0.128.

### *Simulation of Monomolecular Cracking*

To simulate a monomolecular cracking process, the $A_2$ parameter of the model is set to zero. The results of the simulation shown in Fig. 1 demonstrate the influence of the adsorption parameter, $B$, on the average conversion versus time on stream at a catalyst-to-reactant ratio of 0.128. The total activity of the catalyst, as represented by the monomolecular rate constant, is 1 (i.e., $k_M = 1$) for all curves. The $B$ parameter was varied from $-0.99$, corresponding to a ratio of $K_A/(2K_P) = 0.01$, to zero, corresponding to the observed first-order kinetic model if $K_A = 2K_P$. If $N$ is varied, the curves exhibit the three classes of decay described previously (*23*). These are determined solely by the value of the decay exponent, $N$. With $N = 1$, the curves are monotonic and approach an asymptotic value of average conversion as time on stream is increased. From Fig. 1, it can be seen that as competitive inhibition by the products is increased ($B$ approaching $-1$) the average conversion obtained is significantly reduced for a given set of conditions. Under severe inhibition ($B = -0.99$) average conversion is almost constant after 5 time units, while at $B = 0$ a longer time on stream is required to arrive at a much higher asymptote.

Figure 2 shows the effect of the decay rate parameter $G$ on the first order model ($A_2$ and $B = 0$). Catalytic activity is the same as in Fig. 1. It can be seen that as $G$ is

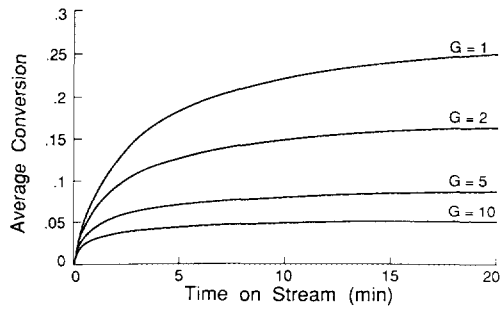


FIG. 2. Monomolecular model simulations: decay effects; $G$ as indicated; $B = 0$; other parameters as in Fig. 1.

increased, the average conversion obtained for a given set of conditions is reduced in a manner which is qualitatively quite similar to the effect of increasing competitive inhibition. Discrimination between these two effects is made possible only by obtaining data at a wide range of catalyst-to-reactant ratios and applying Eq. (10). Even so, the combined effects of experimental error and decay rate could make discrimination between the two phenomena difficult.

*Simulation of Chain Cracking*

In a system where chain cracking is kinetically significant, the $A_2$ parameter will be negative and smaller in magnitude than $A_1$. The sum of these two parameters is related to the contribution of monomolecular protolysis to the total conversion and cannot be zero since it accounts for the initial source or carbenium ions. In principle, however, carbenium ions could come from any source such as added olefins or olefins from thermal reactions, as was suggested by Weisz (*24*). Simulations were conducted using a series of $A_2$ values while keeping the total "intrinsic activity" constant ($k_M + k_C = 1$) in order to investigate if there are observable effects on conversion when chain reactions are present.

It was found that the value of the $B$ parameter had a strong effect on the morphology of conversion versus time-on-stream plots obtained at any real value of $A_2$, i.e., in the presence of chain processes. This seems to be reasonable since this parameter governs ion concentration on the catalyst surface, thus directly influencing the contribution of chain processes to the overall reaction kinetics. To demonstrate this effect, we first examine the effect of chain processes when the products of reaction are very much more strongly adsorbed on the catalyst than the reactant. To simulate this situation, $B$ was assigned a value of $-0.99$, corresponding to the average adsorption constant on the products being fifty times that of the reactant. Figure 3 presents the simulated average conversion predicted by the model as the activity of the catalyst shifts from a purely monomolecular reaction ($k_M = 1$; $k_C = 0$; lower curve) to one in which chain processes dominate ($k_M = 0.01$; $k_C = 0.99$; upper curve). The conversion versus time on stream curves exhibit purely monotonic behaviour for $k_M = 1$ and an increasingly evident induction period as the mechanism shifts to being dominated by chain reactions ($k_C = 0.99$). The induction period under these adsorption conditions is short due to the rapid shift in the mechanism of conversion to the bimolecular, chain propagation, route. This we ascribe to the high coverage of the surface by carbenium ions which facilitate bimolecular reactions while inhibiting monomolecular processes by reducing the availability of pristine sites for the initiation reaction.

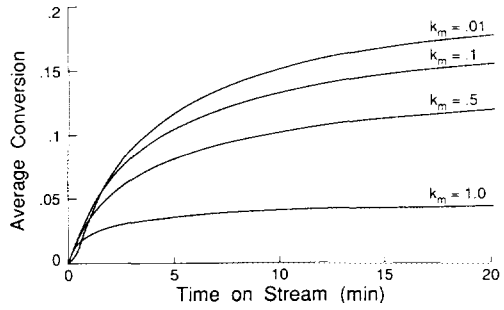


FIG. 3. General model simulations: mechanism effects; $B = -0.99$; $k_M + k_C = 1$; other parameters as in Fig. 1.

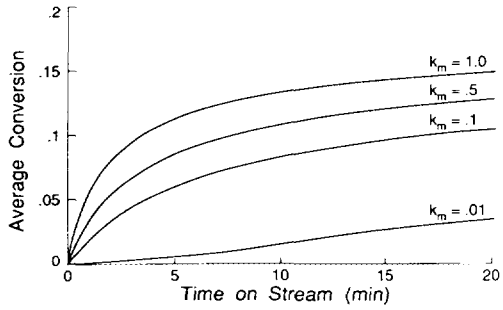


FIG. 4. General model simulations: mechanism effects; $B = -0.75$; $k_M + k_C = 1$; other parameters as in Fig. 1.

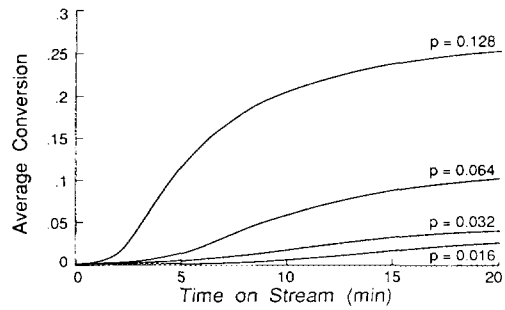


FIG. 6. General model simulations: catalyst to reactant ratio ($P$) effects; $B = -0.0$; $k_M = 0.001$; $k_C = 0.999$; $B = -0.5$; other parameters as in Fig. 1. $P$ is the catalyst to reactant weight ratio.

Simulations of the case where the reactant competes for adsorption sites more successfully are presented in Figs. 4 and 5. The values of the $B$ parameter are $-0.75$ and $-0.50$, respectively. The induction period and acceleration due to the change in the relative importance of the two mechanisms is more gradual as $B$ increases. The difference in morphology between in Figs. 4 and 5 and Fig. 3 is exclusively due to changes in adsorption constants, since all other parameters, including the sum of the two rate constants, are the same. When products and reactants compete more equally for the adsorption sites, a higher concentration of product olefins in the gas phase is required to effect the change in mechanism. The result is that the induction period is more gradual and the acceleration

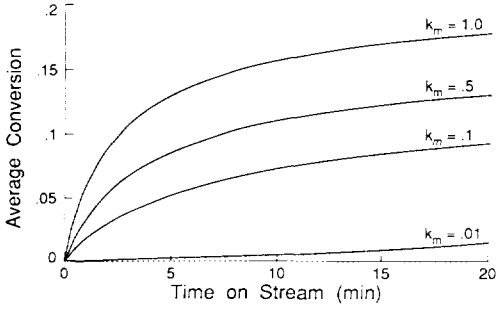


FIG. 5. General model simulations: mechanism effects; $B = -0.5$; $k_M + k_C = 1$; other parameters as in Fig. 1.

more evident in practice. This effect is accentuated in Fig. 6, where the catalyst-to-reactant ratio is varied in a system where chain processes account for 99.9% of the activity and $B = 0$. The morphology observed here is similar to that previously reported with for the cracking of $C_6$ paraffins (*25*). Interestingly, as the catalyst-to-reactant ratio increases, the induction period seems to become shorter. This is due to the fact that a certain level of conversion is required to saturate the surface with carbenium ions derived from product olefins and hence to make chain cracking dominant. This level of conversion is reached at a shorter time on stream for high cat/oil runs. The resultant behaviour of the constant cat/oil plot is such that the induction period is over at a shorter time on stream.

To confirm the generality of this behaviour a system whose kinetics are dominated by the chain process but using a decay exponent ($N$) greater than one, was studied. The conversion versus time curve obtained is presented in Fig. 7 and exhibits an initial induction period, an acceleration as the chain mechanism gains in importance, and finally as asymptotic decrease to zero as time increases to infinity. Significantly different parameters were used in this simulation in order to accentuate these phenomena.

It is important to remember that the plots

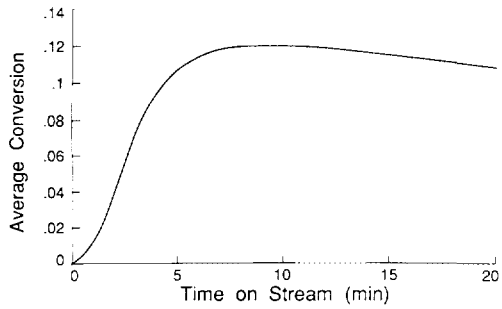


FIG. 7. General model simulation: decay exponent effect; $A_1 = 2$; $A_2 = -1.99$; $B = 0$; $G = 1$; $N = 2$; $\in = 1$.

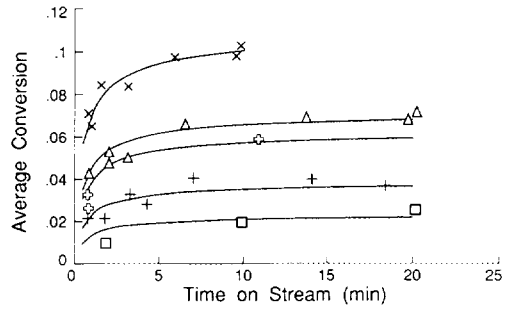


FIG. 8. Fitted data: *n*-nonane on USHY at 673 K. Solid lines represent values predicted using optimal model parameters from Table 1. Catalyst/reactant ratios are: (X) 0.0447, (△) 0.0266, (✥) 0.0180, (+) 0.0091, and (□) 0.0045. $A_2$ and $N$ fixed at 0 and 1, respectively.

of fractional average conversion versus time on stream presented in Figs. 1 to 6 represent systems whose total catalytic activity as measured by $k_M + k_C$, is the same in all cases, yet the observed results are dramatically different. Normally, a standard set of conditions is used for screening catalysts, e.g., the ASTM microactivity test. In light of the above simulations, it is evident that such tests do not measure catalytic activity in any fundamental sense but rather some unknown combination of the adsorption, activity, and decay characteristics of the system. The sensitivity of the conversion vs TOS morphology is important to note, since adsorption could differ significantly from catalyst to catalyst due to variations in pretreatment or if novel formulations are being tested. More emphasis and understanding of adsorption equilibria seems to be needed in the study of catalytic cracking. We should also note that the adsorption involved here is the formation of carbonium ions ($K_A$) or carbenium ions ($K_P$), not simply physical adsorption.

### *Testing the Model Using Data from n-Nonane Cracking at 673 K*

The results of fitting the above kinetic model, with $A_2$ fixed at zero, to the cracking data of *n*-nonane at 673 K are presented in Table 1. The fit of the three-parameter model was found to be excellent without any strong correlations between the nonlinear parameters. Attempts to fit a simpler model with both $A_2$ and $B = 0$ were unsuccessful. Figure 8 shows the experimentally determined fractional average conversion versus time on stream for this system, as well as curves representing the optimal fit of the data. Residuals for this fit are plotted against time on stream and catalyst-to-reactant ratio in Figs. 9 and 10, respectively. The value of $N$, the decay exponent, was fixed at one, since the average conversion obtained exhibited asymptotic behaviour as time on stream was increased along a contour of constant catalyst-to-reactant ratio (*23*). The fit, as shown in Figs. 8 to 10 is excellent and is significant at the 95% confi-

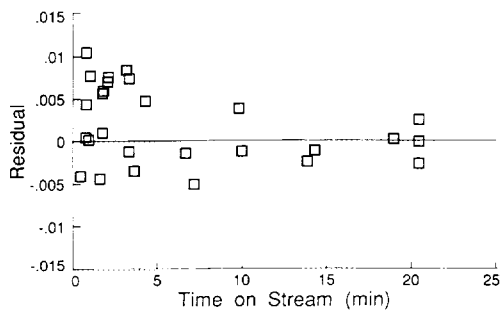


FIG. 9. Residuals versus time on stream for fit of *n*-nonane data at 673 K by model with $A_2$ and $N$ fixed at 0 and 1, respectively.

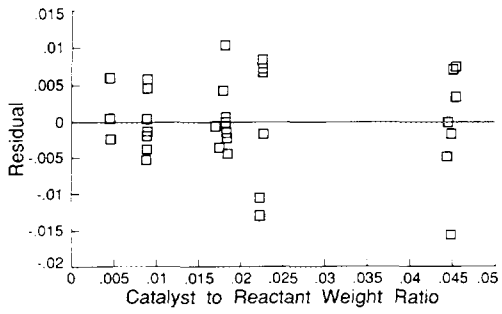


FIG. 10. Residuals versus catalyst to reactant ratio for fit of *n*-nonane data at 673 K to model with $A_2$ and $N$ fixed at 0 and 1, respectively.

dence interval based on a mean-squared experimental error estimate of 4.9E-5 determined from nine replicate runs.

Despite this, mechanistic studies and product selectivity studies (to be described elsewhere) lead to the conclusion that a bimolecular reaction is present in the *n*-nonane system. The minimum initial contribution to total conversion by the bimolecular reaction was found to be 16.5% at 673 K (*26*). Yet an adequate fit of the three-parameter kinetic model indicates that the $A_2$ parameter, which in this development contains all the bimolecular cracking rate constants, is not required to model the overall kinetics. To investigate this unexpected result, the $A_2$ parameter was freed and again optimal parameters were obtained. It was found that the $A_2$ parameter was indeed not significant at the 95% confidence interval using the principle of extra sum of squares of residuals.

Upon further investigation, it was found that a large number of combinations of $A_1$ and $A_2$ values, requiring relatively small adjustments of the $B$ and $G$ gave the same or very close to the same sum of squares of residuals (SSR), when fitting the data. The combinations of $A_1$ and $A_2$ which settle at the minimum in the sum of squares of residuals consist of sets where $A_1 + A_2$ was approximately constant. To pursue this matter further, average conversion data were synthesized using the experimental conditions (catalyst-to-reactant ratios, times on stream) of the *n*-nonane data set for a series of $A_1$ and $A_2$ values with $A_1 + A_2$, $B$, $G$, and $N$ held constant at values listed in Table 2. The values of $A_1$ and $A_2$ used represented systems where between 0 and 90% of the catalytic activity stemmed from bimolecular processes as measured by the ratio of $|A_2|$ to $A_1$. Gaussian noise with variance equal to that of the *n*-nonane data was then added to the synthesized data points, and the three-parameter model fitted to the resulting synthetic data set. Table 3 illustrates

TABLE 2

Kinetic Parameters: *n*-Nonane at 673K

| | Temp. (K) | $A_1$ $\left(\frac{\text{mol}}{\text{g cat min}}\right)$ | $B$ | $G$ (min$^{-1}$) | $N$ |
|---|---|---|---|---|---|
| | 673 | 0.694 | −0.932 | 5.511 | 1.0[a] |
| | Approx std. error | 0.019 | 0.004 | 0.093 | 0.0 |
| Correlation matrix: | | | | | |
| | | $A_1$ | $B$ | G | |
| $A_1$ | | 1.000 | | | |
| $B$ | | 0.784 | 1.000 | | |
| $G$ | | 0.709 | 0.184 | 1.000 | |

[a] The decay exponent was fixed at one since our data exhibit asymptotic behaviour as time on stream becomes large.

TABLE 3

Monte Carlo Simulation Results

| | 50%[a] | | 75% | | 90% | |
|---|---|---|---|---|---|---|
| | Sim[b] | Fitted[c] | Sim | Fitted | Sim | Fitted |
| $A_1$ | 1.388 | 0.755 | 2.775 | 0.871 | 6.938 | 1.265 |
| $A_2$ | −0.694 | 0.000 | −2.081 | 0.000 | −6.244 | 0.000 |
| $B$ | −0.932 | −0.915 | −0.932 | −0.910 | −0.932 | −0.840 |
| $G$ | 5.211 | 4.926 | 5.211 | 4.467 | 5.211 | 2.657 |
| $F$ (value) | | 1.136 | | 1.398 | | 1.820 |

[a] Percentages represent $(-A_2/A_1) \times 100$. Sum $A_1 + A_2 = 0.694$ in all cases.

[b] SIM represents the parameter values used to synthesize the data set.

[c] Optimal parameters obtained by fitting a three-parameter model to simulated data generated by the parameters shown and containing Gaussian noise as described in the text.

the results of this Monte Carlo type procedure for simulated data sets of 50, 75, and 90% catalytic activity due to bimolecular processes. It was found that for systems where bimolecular processes accounted for less than 90% of the catalytic activity, the three-parameter model was statistically significant at the 95% confidence level. For the system with 90% activity from chain processes, the three-parameter model is still adequate according to the $F$-ratio test, however, trends appear in the residuals with respect to P, the catalyst-to-reactant weight ratio, and to $\overline{X}_f$, the conversion. We conclude that at our reaction conditions and using the described methodologies, chain processes could account for up to 90% of the catalytic activity without adversely influencing the fit of the three-parameter model. Further simulations showed that if the decay rate or experimental error had been lower, the influence of chain reactions on the total rate of reaction could have been more easily assessed.

### *Application of the Model to Data from 2-Methylpentane Cracking*

Previously published data from the cracking of 2-methylpentane, which exhibits sigmoidal curves of average conversion versus time on stream (9), have been fitted to the kinetic model proposed here. The model was found to be an inadequate representation of the data. This is clearly illustrated by the residual plot of Fig. 11 for the data of 2-methylpentane against time on stream. A distinct trend in the residuals plotted against time on stream is observed. Since in addition to catalytic reactions, thermal reactions are also known to be present in this data, a trend is to be expected in the residuals with respect to time (27). To account for these thermal reactions, the model should be modified to account for conversion due to thermal reactions or thermal conversion should be subtracted from the total measured conversion. It is reassuring to find that in the case of a known abberation in the data the model clearly indicates that a problem exists. This

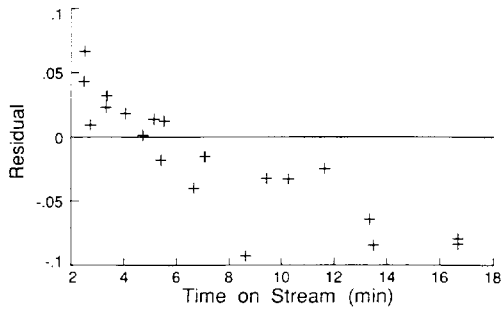


FIG. 11. Residual plot for 2-methylpentane data against time on stream. Lack of fit of model.

TABLE 4

Optimal Parameter Estimates: *n*-Paraffins[a]

| Reactant | Catalyst[b] | Temperature | $A_1$ $\left(\frac{\text{mol}}{\text{g cat min}}\right)$ | $B$ | $G$ (min$^{-1}$) | Ref. |
|---|---|---|---|---|---|---|
| *n*-Hexane | A | 773 | 0.492 | −0.759 | 1.62 | (*5*) |
| *n*-Heptane | B | 703 | 0.096 | −0.995 | 1.32 | (*18*) |
| *n*-Octane | A | 673 | 0.072 | −0.977 | 1.10 | (*5*) |
| *n*-Nonane | C | 673 | 0.694 | −0.932 | 5.51 | (*2*) |
| *n*-Nonane | C | 723 | 3.83 | −0.729 | 5.14 | |
| *n*-Nonane | C | 763 | 10.8 | −0.471 | 4.90 | |
| *n*-Dodecane | A | 673 | 0.304 | −0.984 | 0.991 | (*5*) |
| *n*-Dodecane | D | 673 | 0.219 | −0.958 | 0.985 | (*19*) |

[a] The decay exponent, $N$, was fixed at one, since the experimental data exhibit asymptotic behaviour as time on stream increases along a contour of constant catalyst-to-reactant ratio. The model was found to be significant at the 95% confidence interval for each system.

[b] Catalysts: (A) 97% Exchanged USHY, (B) 15% exchanged LaHY, (C) 99% exchanged USHY, and (D) LaY unspecified properties.

assures us that the model is not infinitely flexible and able to fit erroneous results.

### *Application of the Model to Data from n-Alkane Cracking*

The results of fitting the kinetic model, with $A_2$ set at zero, to the cracking data for *n*-hexane (*15*), *n*-heptane (*12*), *n*-octane (*11*), and *n*-dodecane (*25*) from the literature and *n*-nonane from this study are presented in Table 4. For all data sets the fit of the three-parameter model was excellent. Attempts to fit the simpler first-order kinetic models ($A_2$ and $B = 0$) were unsuccessful. The decay exponent $N$ was assigned in all cases a value of one, since the average conversion data exhibit asymptotic behaviour as time on stream is increased along contours of constant catalyst-to-reactant ratio (*23*). The fit for each system was found to be significant at the 95% confidence interval based upon a variance estimate of 4.9E-5 determined from nine replicate runs in the *n*-nonane experiments. The fitted fractional average conversion data for the *n*-nonane system at three temperatures are presented in Figs. 12, 13, and 14. The $A_2$ parameter was found to be statistically insignificant for all systems examined, thus the influence of bimolecular cracking is not detectable in these systems via kinetic analysis alone. This parametric insensitivity was discussed above in detail for the 673-K data. Similar analysis of the *n*-nonane data at 723 and 763 K showed that the maximum possible contribution by chain processes to the overall kinetics, without adversely affecting the fit of the three parameter model, are 70 and 45% respectively. These figures are related to the value of the $B$ parameter, suggesting that sensitivity of the fit to the value of $A_2$ is associated with the relative

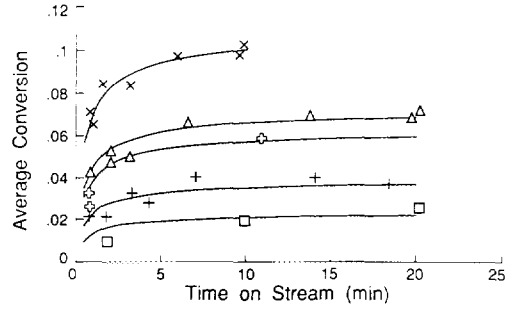


FIG. 12. Fitted data for *n*-nonane on USHY at 673 K. Solid lines represent predicted values. Catalyst-to-reactant weight ratios are: (x) 0.0477, (△) 0.0266, (✣) 0.0180, (+) 0.091, and (□) 0.0045.

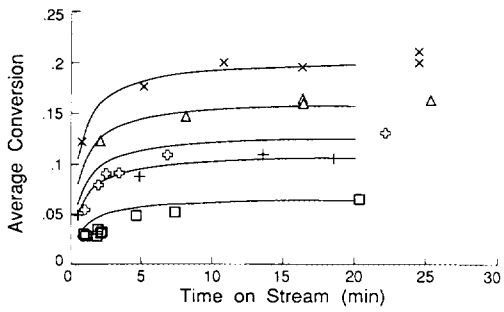


FIG. 13. Fitted data for *n*-nonane on USHY at 723 K. Solid lines represent predicted values. Catalyst-to-reactant weight ratios are: (x) 0.0477, (△) 0.0266, (◈) 0.0180, (+) 0.091, and (□) 0.0045.

values of the equilibrium adsorption constants for the reactant and products.

The *n*-heptane data had been previously modelled using a first-order model ($A_2 = B = 0$). We found that this model did not give a satisfactory fit of the data. Based upon the principle of extra sum of squares, the $B$ parameter was found to be statistically significant at the 95% confidence interval with an optimal value $-0.9995$.

The values of the optimal parameters reported for *n*-hexane, *n*-octane, and *n*-dodecane data differ somewhat from those reported previously though not enough to alter previously stated conclusions. These differences are attributed to the increased accuracy of the numerical methods used in this study. The previously published parameter estimates were obtained as follows:

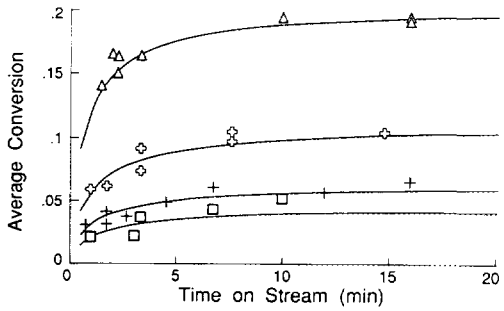


FIG. 14. Fitted data for *n*-nonane on USHY at 763 K. Solid lines represent predicted values. Catalyst-to-reactant weight ratios are: (x) 0.0477, (△) 0.0266, (◈) 0.0180, (+) 0.091; and (□) 0.0045.

The predicted average conversion was determined by numerically integrating the differential rate expression with respect to space time, $\tau$, using Hamming's predictor corrector method (*23*) at five nodes between $t = 0$ and $t = t_f$ regardless of the values of the parameters or the time on stream, $t_f$. These five numerically determined values of $X_f$ were then used as the function values in a quadrature integration with respect to time on stream to obtain a value for the time averaged conversion, $\bar{X}_f$. In the current work, the instantaneous conversion was determined by finding the roots of the implicit equation in $X_f$ at five nodes for each step in time. These values were then used in a five-step Gaussian quadrature integration to calculate $\bar{X}_f$. The step size taken in the time domain was selected to ensure the error in each step did not exceed a prescribed tolerance. Thus the methodology in this study replaces Hamming's numerical integration routine with respect to space time by a root finding procedure of arbitrary accuracy ($X_f$ was determined to an accuracy of 1.E-8) and improves the accuracy of the numerical integration in the on stream time domain by an appropriate step control policy.

The optimal parameters for the various paraffin systems can be analyzed to yield information about the rate and equilibrium adsorption constants of the system using the values presented in Table 5. Consider for example the effect of temperature on the adsorption parameter $B$ in *n*-nonane cracking.

Given only the optimal values of the $B$ parameter, it is evident that individual equilibrium adsorption constants of the system cannot be determined. It is however possible to derive useful information from the temperature dependence of this parameter. This we do by examining the two limiting cases;

TABLE 5

Parametric Analysis: *n*-Paraffins

| Feed | Temp. (K) | Catalyst[c] | lim $\sum K_i \mathcal{F}_i \gg 1$[a] | | lim $\sum K_i \mathcal{F}_i K_A^b$ | |
|---|---|---|---|---|---|---|
| | | | $K_P/K_A$ | $\sum k_i[S_0]$ | $K_P$ | $\sum k_i[S_0]K_A$ |
| *n*-Hexane | 773 | A | 2.27 | 0.0237 | 109.0 | 2.04 |
| *n*-Heptane | 703 | B | 105.0 | 0.192 | 6041.0 | 19.3 |
| *n*-Octane | 673 | A | 22.3 | 0.0275 | 1201.0 | 3.13 |
| *n*-Nonane | 673 | C | 7.35 | 0.0937 | 379.0 | 10.2 |
| *n*-Nonane | 723 | C | 1.78 | 0.110 | 77.0 | 14.1 |
| *n*-Nonane | 763 | C | 0.88 | 0.159 | 25.9 | 20.4 |
| *n*-Dodecane | 673 | A | 27.7 | 0.114 | 1507.0 | 19.3 |
| *n*-Dodecane | 673 | D | 10.4 | 0.0306 | 548.0 | 5.22 |

[a] High product coverage assumption: $K_A/\bar{K}_P$ calculated according to Eq. (9). $\sum k_i[S_0]$ calculated according to Eq. (13).

[b] Low reactant coverage assumption: $\bar{K}_P$ and $\sum k_i[S_0]K_A$ calculated according to Eqs. (12) and (15), respectively.

[c] Catalyst types are as in Table 4.

(1) $\sum K_i \mathcal{F}_i C_{A_0} \gg 1$, i.e., the system is in the region of high surface coverage by the products of reaction, and;

(2) $\sum K_i \mathcal{F}_i \gg K_A$, which only assumes that the products are adsorbed much more readily than the reactant.

To proceed with the analysis, a weighted average equilibrium constant for the products of cracking, $\bar{K}_P$, is defined as follows:

$$\bar{K}_P = \frac{\sum K_i \mathcal{F}_i}{\sum \mathcal{F}_i}. \tag{17}$$

Since the initial product distribution for *n*-nonane consists predominantly of $C_4$ and $C_5$ fragments and is fairly constant over the temperature range (*26*), calculation of an average quantity such as that defined by $\bar{K}_P$ seems to be justified.

An expression which governs the ratio of $\bar{K}_P$ to $K_A$ can be obtained by solving for $K_A$ and dividing by $\bar{K}_P$. This results in

$$\frac{K_A}{\bar{K}_P} = \frac{K_A \sum \mathcal{F}_i}{\sum K_i \mathcal{F}_i} = (B + 1)\left(\sum \mathcal{F}_i + B/(C_{A_0}\bar{K}_P)\right). \tag{18}$$

Using the high coverage assumption (assumption 1) from Eq. (18) we get

$$\frac{K_A}{\bar{K}_P} \cong (B + 1) \sum \mathcal{F}_i. \tag{19}$$

Rearrangement of Eq. (13) can also yield

$$\bar{K}_P = \frac{\sum K_i \mathcal{F}_i}{\sum \mathcal{F}_i} = \frac{1}{(B + 1)(\sum \mathcal{F}_i)}\left[K_A - \frac{B}{C_{A_0}}\right]. \tag{20}$$

Under assumption 2 (preferential product adsorption), Eq. (20) simplifies to

$$\bar{K}_P = \frac{\sum K_i \mathcal{F}_i}{\sum \mathcal{F}_i} \cong \frac{-B}{(B + 1)(\sum \mathcal{F}_i)C_{A_0}}. \tag{21}$$

Based upon assumption 1, the optimal values of the $B$ parameter give ratios of the adsorption constant of the reactant to the weighted average adsorption constant of the products of 0.136, 0.562, and 1.140 and 673, 723, and 763 K, respectively, suggesting that the reactant competes for adsorption sites more successfully at high reaction temperatures. Alternatively, analysis via assumption 2 yields weighted average equilibrium adsorption constants of the prod-

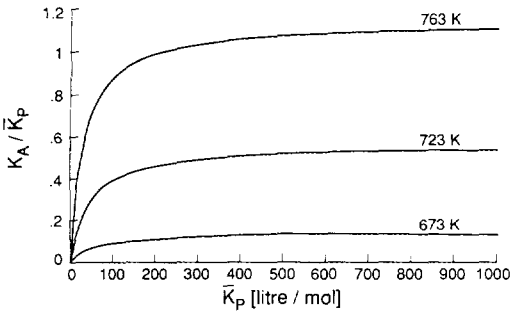


FIG. 15. Ratio of the equilibrium adsorption constant of the reactant, $K_A$, to that of the weighted average product, $K_P$, plotted as a function of $K_P$ along contours of constant $B$ for $n$-nonane data. $B$ = −0.9323, −0.7292, and −0.4706 at 673, 723, and 763 K, respectively. Contours are calculated based on Eq. (9).

ucts of 379., 77.0, and 25.9 [litre/mole] at 673, 723, and 763 K, respectively, using Eq. (21). This second approach suggests that a rapid decrease in surface coverage by products occurs, but does not yield information about reactant adsorption since it is assumed to be negligible relative to that of the products.

Using Eq. (18) and the ideal gas law, the ratio of the adsorption constants at the three temperatures as determined in this way is presented in Fig. 15. Each curve follows a contour of constant $B$ (set at the experimental value) for the system. Any point on a curve yields a set of coordinates $\bar{K}_P$ and $K_A/\bar{K}_P$ which are a possible solution for the $n$-nonane system at the temperature indicated. As the value of $\bar{K}_P$ increases, the ratio $K_A/\bar{K}_P$ approaches that predicted by assuming $\sum K_i \mathcal{F}_i C_{A_0} \gg 1$ (assumption 1). Since the high product coverage assumption yields information based on taking the limit as $\bar{K}_P$ goes to infinity, it also implies significant surface coverage by reactant.

Figure 16 presents the calculated value of $\bar{K}_P$ for various values of $K_A$ according to Eq. (20) along contours at constant $B$ for that temperature. It can be seen that the values obtained for $\bar{K}_P$ in the limit, as $K_A$ approaches zero, are consistent with those obtained by assuming that $\sum K_i \mathcal{F}_i \gg K_A$ (assumption 2), where the reactant is in the low coverage region. In this case, $\sum K_i \mathcal{F}_i C_{A_0}$ will be 14, 3, and 1 at 673, 723, and 763 K, respectively. Surface coverage by products is then sparse at higher reaction temperatures only.

Unfortunately there is no evidence to show if either of these assumptions is representative of this system over the temperature range used. The results from the fitting of the kinetic model to the data from $n$-octane and $n$-dodecane on an USHY catalyst give estimates of $B$ which are very close to −1. This can only occur if these systems are in the high surface coverage region and the products are much more strongly adsorbed than the reactant. Since the $n$-nonane results were obtained on a different USHY catalyst and because adsorption effects of catalysts are sensitive to pretreatment conditions, it cannot be assumed that a high coverage situation exists in the present study as well.

Although it cannot be unequivocally determined where on Figs. 15 or 16 this system lies, the Van't Hoff relationship (*28*), which describes the temperature dependence of equilibrium constants, can be used to obtain differences in enthalpies of adsorption between products and reactant. The observed difference in enthalpy of adsorption, $\Delta\Delta H$, was determined from the slope of the logarithm of the ratio of $K_A/\bar{K}_P$ against inverse temperature for various val-

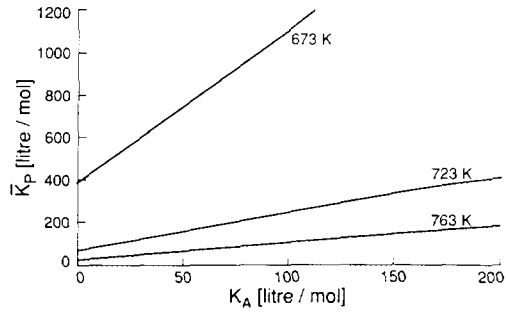


FIG. 16. Relationship between $K_P$ and $K_A$ along contours of constant $B$ as governed by Eq. (11) for $n$-nonane data. $B$ parameter as in Fig. 4.

ues of $\overline{K}_P$. Such analysis predicts that $\Delta\Delta H$ ($= \Delta H_P - \Delta H_A$) is 30.45 kcal/mol (low reactant coverage assumption 2) and 24.32 kcal/mol (high coverage assumption 2). The two values of $\Delta\Delta H$ represent the minimum and maximum differences in enthalpy of adsorption between the reactant and the average product. It is apparent that at higher temperatures the reactant will compete for adsorption sites much more successfully under either assumption. In a similar fashion the behaviour of the sum of the monomolecular rate constants can be analyzed. Using Eq. (11), (12), and (13), $\sum k_{M_i}[S]_0$ can be obtained as a function of the parameters of the system and $K_A$ for the completely general case shown below:

$$\sum k_{M_i}[S]_0 = \frac{A_1 + A_2}{B + 1}\left(\frac{1}{K_A + C_{A_0}}\right). \quad (22)$$

Under the assumption of high reactant surface coverage ($K_A \gg 1$), Eq. (22) simplifies to

$$\sum k_{M_i}[S]_0 = \frac{A_1 + A_2}{B + 1} C_{A_0}, \quad (23)$$

while under the low reactant surface coverage assumption Eq. (11), (12), and (13) give

$$\sum k_{M_i} K_A [S]_0 = \frac{A_1 + A_2}{B + 1}. \quad (24)$$

Since $K_A$ approaches zero for this assumption, it must be included in the left-hand side of Eq. (24). Figure 17 presents $\sum k_{M_i}[S]_0$ using the optimal parameters obtained for *n*-nonane at the three temperatures investigated as a function of assumed values of $K_A$ using Eq. (22). Using the high reactant coverage assumption we obtain an average activation energy, $E_{obs}$, of 6.3 kcal/mol with a linear correlation coefficient of 0.986. The low reactant coverage assumption predicts $E_{obs}$ 7.7 kcal/mol with a linear correlation coefficient of 0.990. The observed activation energies of reaction were found to be independent of the assumed enthalpy of adsorption of the reactant.

The observed "activation energy" for the cracking reaction is therefore less than

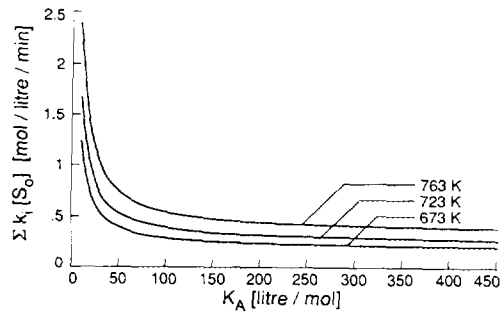


FIG. 17. Predicted values of $\sum K_{M_i}[S]_0$ for *n*-nonane as a function of $K_A$ along contours of constant $B$ based on Eq. (13). $B$ values as in Fig. 4.

1/10 the average C–C bond dissociation energy (81 kcal/mol) (*29*) and much lower than would be anticipated for the true activation energy of cracking. An anomalously low activation energy has also been previously reported in cumene cracking (*30*). Assuming that the enthalpy of adsorption is positive and given that the overall reaction is endothermic by between 12 and 17 kcal/mol, a true activation energy of reaction of 6 to 8 kcal/mol is not possible. Furthermore, bulk diffusional restrictions were ruled out as the rate-limiting step by verifying that catalyst particle size had no influence on the conversion obtained (*26*). In published work on cumene cracking, Best and Wojciechowski (*30*) made the case that the formation of a carbenium ion from cumene is an endothermic process. The same situation may exist here.

*Bond Cracking Probability*

By applying the two limiting coverage assumptions to the parameters obtained for the reactions of *n*-octane, *n*-nonane, and *n*-dodecane, the effect of carbon chain length on reaction kinetics can be investigated. Selectivity data for *n*-octane and *n*-dodecane indicate that the smallest fragment formed in the initial reactions was a $C_3$ fragment (*25*). Thus there are three and seven C–C bonds which can react in the *n*-octane and *n*-dodecane molecule, respectively. The selectivity data for *n*-nonane (*26*) re-

TABLE 6

Influence of Carbon Chain Length[a]

| Reactant | C.B.[b] | lim $K_A \gg 1$ | lim $\Sigma K_i \mathcal{F}_i \gg K_A$ | |
|---|---|---|---|---|
| | | $\frac{\Sigma k_i [S_0]}{\text{C.B.}}$ | $\frac{\Sigma k_i [S_0] K_A}{\text{C.B.}}$ | Corrected[c] |
| *n*-Octane | 3 | 0.0092 | 1.05 | 1.05 |
| *n*-Nonane | 6 | 0.0156 | 1.71 | 1.59 |
| *n*-Dodecane | 7 | 0.0162 | 2.77 | 1.93 |

[a] Calculations were based on parameters in Table I for *n*-octane and *n*-dodecane on catalyst A and *n*-nonane on catalyst C using Eq. (14) and (15) for the high and low reactant coverage assumptions using results at 673 K.

[b] C.B. indicates the number of crackable bonds.

[c] This column represents the normalized cracking rate for the low reactant coverage limit, assuming the reactant adsorption constant increases in proportion to the reactant molecular size.

veals the presence of $C_2$, and $C_7$ fragments as initial products, thus there are six "crackable" C–C bonds in this system. Dividing the values of $\Sigma k_{M_i} [S_0] K_A$ and $\Sigma k_{M_i} [S_0]$ obtained from the low reactant and high product coverage assumptions discussed above by the number of crackable bonds yields average cracking rates per crackable bond. The results are presented in Table 6. Under the low reactant coverage assumption, an additional relationship is required between the reactant adsorption constants for the various feed molecules. It has been previously reported that the adsorption constant of a linear paraffin on a zeolite increases linearly with increased carbon chain length (*31*). Thus the adsorption constant of *n*-octane was assigned a value of 1, and those of *n*-nonane and *n*-dodecane were made to increase in proportion to the number of carbon atoms in each molecule. The results of such an analysis are also shown in Table 6.

With either assumption it is found that the normalized cracking rate per crackable bond increases in the series *n*-octane, *n*-nonane, *n*-dodecane, where we have data at 673 K. Interestingly, the rate at which the increase occurs is approximately the same for the two assumptions. Nace (*32*) reported that the observed kinetic rate constant for cracking of *n*-paraffins on HX catalyst increased with carbon number up to $C_{16}$, then decreased. Abbot and Wojciechowski (*25*) reported an increased cracking reactivity per bond for the series *n*-octane, *n*-dodecane, *n*-hexadecane on USHY zeolite. While it is to be expected that the electron distributions for the C–C bonds along the molecule are not identical as one moves toward the centre of the molecule, it would be surprising if these subtle differences can be observed in this type of experiment. One possible explanation lies in the implicit assumption that the bimolecular mechanism makes a negligible contribution to the estimate obtained for the $A_1$ parameter when $A_2$ is found to be statistically insignificant. In fact, the values of the $A_1$ parameter also account for any bimolecular conversion occurring. The observation that our kinetic equation cannot "see" this process is due to the form of the equation and its properties when statistics is applied to test for the adequacy of fit. It is therefore likely that estimates of cracking rate per C–C bond based on $A_1$, or on a first-order constant from an even simpler kinetic expression, are in fact artifacts due to the contributions to cracking activity made by

bimolecular reactions. Such contributions cannot be separated from the monomolecular rate and the interpretation of changes in $A_1$ as being due to monomolecular cracking alone presents a distorted picture.

It appears therefore that reports in previous kinetic studies showing that the cracking rate per crackable bond increases with reactant molecule length are in fact such as artifact caused by the unrecognized contributions of the bimolecular chain process to overall conversion. This in turn suggests on the basis of the results in Table 6 that longer feed molecules are converted to an increasing degree by bimolecular chain processes.

*Catalyst Decay*

The rate of decay in *n*-nonane cracking *decreases* with temperature. We ascribe this to the reduction of surface coverage by carbenium ions, as discussed above. It is the surface ions and their chance malignant reactions which lead to coke and to catalyst decay. In the *n*-nonane reaction a reduction in the adsorption of products (olefins which form carbenium ions) is almost exactly balance by the increase in rate due to the temperature coefficient (activation energy effect) of the malignant reactions, so that the net result is a small decrease in the rate of decay. Such a balancing act will clearly allow increases or decreases in decay rates, depending on the molecule and even the catalyst being investigated.

## CONCLUSIONS

A general kinetic model and a numerical method by which it can be fitted to average conversion data in pure hydrocarbon cracking has been presented. The model encompasses previously proposed kinetic models and accounts for most of the currently postulated mechanisms of catalytic cracking. The model has been shown to be applicable to experimental data on the cracking of a variety of paraffins on USHY, though it appears to lack an appropriate time component to describe previously published cracking data for 2-methylpentane, which is known to include thermal conversion.

The influence of the chain mechanism on reaction kinetics can be masked by various phnomena. Fitting of simulated data generated by a four-parameter model which encompasses both monomolecular and chain cracking mechanisms indicates that the chain process could account for up to 90% of the catalytic activity in the *n*-nonane system and still not influence the ability of a three-parameter model to describe the kinetics adequately. Experimental error, the high rate of catalyst decay, the necessity to work with average conversion data, and perhaps some of the simplifications in the model contribute to model insensitivity to chain-mediated cracking reactions. If the decay rate had been larger, even the effects of adsorption would be difficult to discern, and a two-parameter model may well be found to be statistically adequate to describe our data. To define the true mechanism of reaction, detailed studies of product selectivity will in general be necessary.

The model has been shown to be applicable to the reactions of linear paraffins between $C_6$ and $C_{12}$ on several Y-zeolite catalysts. Extensive data for *n*-nonane show that coverage and composition of the catalyst surface changes significantly between 673 and 763 K, due to a large difference in the enthalpy of adsorption between the products and the reactant.

An anomalously low activation energy was obtained for this cracking reaction. This low value may be the result of the influence of chain cracking processes on the first-order $A_1$ parameter or to endothermic adsorption in the process of formation of carbonium ions.

The cracking rate per crackable bond, assuming only monomolecular cracking, was found to increase over the range of linear paraffins examined. This is believed to be an artifact due to the effect of an unrecognized contribution of chain processes to the total first-order catalytic activity, and to the fact that linear paraffins of different chain

length have a different tendency to crack by chain processes.

We conclude that adsorption equilibria play a major role in catalyst activity and selectivity. Our model distinguishes between the effects of adsorption decay and of site activity as described by the $B$, $G$, and $A_1$ parameters. It is, however, unable in the case of $n$-alkanes to distinguish between monomolecular and bimolecular rates of reaction from kinetic data alone.

## REFERENCES


1. Lombardo, E. A., and Hall, W. K., *J. Catal.* **112,** 565 (1988).
2. Haag, W. O., and Dessau, R. M., *in* "Proceedings, 8th International Congress on Catalysis, Berlin, 1984" Vol II, p. 305. Decherma, Frankfurt-am-Main, 1984.
3. Abbot, J., and Wojciechowski, B. W., *in* "Proceedings, 9th International Congress on Catalysis, Calgary, 1988" (M. J. Phillips and M. Ternan, Eds.), Vol. I, p. 206. Chem. Institute of Canada, Ottawa, 1988.
4. Abbot, J., and Wojciechowski, B. W., *Can. J. Chem. Eng.* **66,** 825 (1988).
5. Corma, A., and Wojciechowski, B. W., *Catal. Rev. Sci. Eng.* **24,** 1 (1982).
6. Pansing, W. F., *J. Phys. Chem.* **69,** 392 (1965).
7. Voge, H. H., *in* "Catalysis" (P. H. Emmett, Ed.) Vol. I, Chap. 5. Reinhold, New York, 1958.
8. Pantcherkoff, B. M., *J. Chem. Phys.* **51,** 740 (1954).
9. Abbot, J., and Wojciechowski, B. W., *J. Catal.* **115,** 1 (1989).
10. Abbot, J., and Wojciechowski, B. W., *J. Catal.* **109,** 274 (1988).
11. Abbot, J., and Wojciechowski, B. W., *J. Catal.* **107,** 451 (1987).
12. Corma, A., Monton, J. B., and Orchilles, A. V., *Appl. Catal.* **23,** 255 (1986).
13. McVicker, G. B., Kramer, G. M., and Ziemiak, J. J., *J. Catal.* **83,** 286 (1983).
14. Lombardo, E. A., Pierantozzl, R., and Hall, W. K., *J. Catal.* **110,** 171 (1988).
15. Abbot, J., and Wojciechowski, B. W., *Can. J. Chem. Eng.* **66,** 817 (1988).
16. Viner, M. R., and Wojciechowski, B. W., *Can. J. Chem. Eng.* **60,** 127 (1982).
17. Haag, W. O., Dessau, R. M., and Lago, R. M., *Stud. Surf. Sci. Catal.* **60,** 255 (1991).
18. White, M. G., "Heterogeneous Catalysis." Prentice-Hall, Englewood Cliffs, NJ, 1990.
19. Levenspiel, O., "Chemical Reaction Engineering," 2nd ed. Wiley, New York, 1972.
20. Brent, R. P., *in* "Algorithms for Minimization without Derivatives." Prentice-Hall, Englewood Cliffs, NJ, 1973.
21. Verner, J., private communication.
22. Press, W. H., Flannery, B. P., Teukolsky, S. A., and Vetterling, W. T., "Numerical Recipes: The Art of Scientific Programming." Cambridge Univ. Press, Cambridge, 1989.
23. Ko, A. N., and Wojciechowski, B. W., *Prog. React. Kinet.* **12,** 201 (1983).
24. Weisz, P. B., *Annu. Rev. Phys. Chem.* **21,** 175 (1970).
25. Abbot, J., and Wojciechowski, B. W., *J. Catal.* **115,** 521 (1989).
26. Groten, W. A., Ph.D. Thesis, Queen's University, Kingston, 1991.
27. Abbot, J., and Wojciechowski, B. W., *J. Catal.* **113,** 353 (1988).
28. Ralston, W., "Mathematical Methods for Digital Computers." Wiley, New York, 1960.
29. Clark, A., "The Theory of Adsorption and Catalysis." Academic Press, New York, 1970.
29. Lowry, T. H., and Richardson, K. S., "Mechanics & Theory in Organic Chemistry." Harper and Row, New York, 1987.
30. Best, D. A., and Wojciechowski, B. W., *J. Catal.* **47,** 343 (1977).
31. Barrer, R. M., and Sutherland, J. W., *Proc. R. Soc. London Ser. A.* **237,** 439 (1956).
32. Nace, D. M., *Ind. Eng. Chem.* **8,** 31 (1969).